JCTC Journal of Chemical Theory and Computation

Article

pubs.acs.org/JCTC

Multiple-Replica Strategies for Free-Energy Calculations in NAMD: Multiple-Walker Adaptive Biasing Force and Walker Selection Rules

Jeffrey Comer,[†,‡] James C. Phillips,[§] Klaus Schulten,[∥,§] and Christophe Chipot*[,†,§,∥]

[†]Laboratoire International Associé Centre National de la Recherche Scientifique et University of Illinois at Urbana−Champaign, Unité Mixte de Recherche No. 7565, Université de Lorraine, B.P. 70239, 54506 Vandoeuvre-lés-Nancy Cedex, France

[‡]Institute of Computational Comparative Medicine and Nanotechnology Innovation Center of Kansas State, Department of Anatomy and Physiology, Kansas State University, Manhattan, Kansas 66506, United States,

[§]Theoretical and Computational Biophysics Group, Beckman Institute for Advanced Science and Technology, University of Illinois at Urbana−Champaign, 405 North Mathews Avenue, Urbana, Illinois 61801, United States

[∥]Department of Physics, University of Illinois at Urbana−Champaign, 1110 West Green Street, Urbana, Illinois 61801, United States

Supporting Information

ABSTRACT: From the most powerful supercomputers to multicore desktops and laptops, parallel computing architectures have been in the mainstream for some time. However, numerical schemes for calculating free energies in molecular systems that directly leverage this hardware paradigm, usually taking the form of multiple-replica strategies, are just now on the cusp of becoming standard practice. Here, we present a modification of the popular molecular dynamics program NAMD that is envisioned to facilitate the use of powerful multiple-replica strategies to improve ergodic sampling for a specific class of free-energy methods known as adaptive biasing force. We describe the software implementation in a so-called multiple-walker context, alongside the interface that makes the proposed approach accessible to the end users. We further evaluate the performance of the adaptive biasing force multiple-walker strategy for a model system, namely, the reversible folding of a short peptide, and show, in particular, in regions of the transition coordinate where convergence of the free-energy calculation is encumbered by hidden barriers, that the multiple-walker strategy can yield far more reliable results in appreciably less real time on parallel architectures, relative to standard, single-replica calculations.

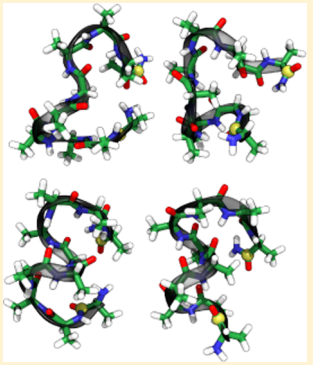

INTRODUCTION

For many-body systems at thermodynamic equilibrium, higher-free-energy microstates receive exponentially less sampling than lower-free-energy states, making equilibrium molecular dynamics simulations unsuitable for determining free-energy changes along transition pathways, especially those possessing energetic barriers larger than the thermal energy. Importance-sampling, or variance-reduction methods, have therefore proven indispensable for computational studies of biomolecular systems.[1,2] A common feature of importance-sampling methods is the requirement to choose a coordinate, or a set of coordinates, that tracks the progress of the system along the transition pathway. Typically, the purpose of importance sampling is to facilitate uniform sampling in the space of these transition coordinates. In the present work, we consider transition coordinates that relate to geometric transformations of the molecular systems, as opposed to the intentionally unphysical transformations used in alchemical free-energy calculations.[3] Comparisons between these different types of transition coordinates can be found elsewhere.[3,4] In the context of geometric free-energy calculations, one usually seeks the potential of mean force along the chosen transition coordinate, that is, the free-energy change as a function of the transition coordinate, with all orthogonal degrees of freedom taking their thermodynamic averages.

It is often implicitly assumed that the transition coordinates capture all slow degrees of freedom and that the orthogonal degrees of freedom rapidly relax, which is required for uniform sampling and convergence of the free energy.[5] Defining coordinates consistent with this assumption of a time scale separation can, however, prove to be a daunting task. In practice, transition coordinates are usually chosen by intuition, notwithstanding developments to aid in their selection.[6] Moreover, there are few guarantees that orthogonal degrees of freedom are appropriately sampled. In many instances, where the choice of the transition coordinate seems trivial, free-energy barriers actually exist along orthogonal degrees of freedom and are rarely traversed during the simulation.[5,7−9] When at least one transition occurs along an orthogonal degree of freedom, careful analysis can diagnose quasi-nonergodicity. In the worst cases, the system remains trapped in a metastable state throughout the simulation, leaving no indication that sampling is poor.[9]

Received: September 30, 2014

   dx.doi.org/10.1021/ct500874p | J. Chem. Theory Comput. XXXX, XXX, XXX−XXX

A straightforward solution to address the issue of appreciable free-energy barriers along orthogonal degrees of freedom, often referred to as hidden barriers,[10] is to fold the offending degrees of freedom into the set of transition coordinates, using importance sampling to eliminate the effects of the barriers.[8] Selecting the appropriate coordinates can, however, prove to be quite difficult, and importance sampling along more than two or three collective variables rapidly becomes computationally intractable.

The performance of importance-sampling schemes can be compared in two ways: (1) the real time required to obtain a sufficiently converged potential of mean force and (2) the computational cost to obtain it. The former is often specified in hours, days, or months, while the latter can be quantified in processor-hours on a given computing architecture, often referred to as "service units" in proposals for supercomputer allocations. Which measure of performance is more important depends on the type of calculation, the nature of the system being simulated, the details of the available computational resources, and the priorities of the researcher. It is often the case that, while a calculation could be performed on a desktop computer at a reasonable computational cost, the real time required might be overwhelming, amounting to years, or simply inconvenient. At these junctures, scientists in the field of molecular simulation turn to highly parallel architectures consisting of hundreds to hundreds of thousands of processing units. While such parallel architectures are well adapted to simulating large molecular assemblies, or many molecular assemblies at once, parellelization in the time domain is difficult. The amount of simulated time per day for a single realization of a system is, therefore, usually reduced to tens to hundreds of nanoseconds—or a few microseconds with specialized hardware.[11]

Due to their inherent parallel structure, multiple-replica paradigms for free-energy calculations, in which multiple realizations of a system are simulated simultaneously, offer a convenient solution to improving sampling, which is at the same time well suited to current trends in computing hardware. Numerical schemes based on multiple replicas can, indeed, alleviate some of the detrimental effects of hidden barriers on sampling without explicitly identifying the associated orthogonal coordinates. Note, however, that multiple-replica schemes do not, by themselves, enhance traversal of hidden barriers, which can, in principle, be accomplished by another class of methods.[10,12,13]

While some advantages could be gained simply by running multiple, independent simulations of similar molecular assemblies, particularly with respect to reducing the real time required for a calculation, dramatic reductions in both real time and computational cost can be obtained by powerful schemes involving on-the-fly communication between replicas.[14−23] Early successes in molecular dynamics associated with multiple-replica techniques employed the parallel-tempering algorithm,[14] which was originally developed in the context of Monte Carlo simulations[24−26] and involves running replicas at different temperatures. Exchange of replicas with different biasing potentials, known as Hamiltonian exchange, or Hamiltonian hopping, alone or in concert with parallel tempering, has also been shown to be particularly effective.[15,16,18,19]

The choice of a multiple-replica paradigm is subservient to the type of importance-sampling algorithm utilized. Here, we focus on one of the several popular approaches to importance sampling, the adaptive biasing force (ABF) algorithm,[5,27,28] which has a number of desirable properties, including, arguably enough, its conceptual simplicity, ease of statistical error analysis,[5,29] and mathematical rigor.[30,31] In a nutshell, the algorithm collects samples of the force at each value of a discretized transition coordinate. The negative of the best estimate of the mean force is then applied to approximately cancel the true mean force, thereby smoothing the ruggedness of the free-energy landscape and eliminating barriers. The calculation ideally progresses as follows—better estimates of the mean force enhance sampling along the transition coordinate, which, in turn, yields better estimates of the mean force, improving further sampling. As the mean force estimates become increasingly accurate, the sum of the intrinsic mean force and the biasing force approach zero, so that the effective free-energy surface along the transition coordinate, or coordinates, becomes flat and is explored by free diffusion. This ideal scenario may be thwarted by hidden barriers along coordinates orthogonal to the transition-coordinate space, which can hamper convergence of the mean force.

In the context of calculations, algorithms employing multiple replicas of the system have been referred to as multiple-walker[21] methods—so-called because each replica executes a random walk along the transition coordinate. First demonstrated by Lelièvre et al.,[32] multiple-walker ABF yields faster convergence and better sampling of orthogonal degrees of freedom,[21,22] relative to a single, long calculation, or a calculation with multiple, independent replicas. However, in the field of scientific computation, many powerful techniques appearing in print go unused, owing to the lack of a convenient implementation in a popular software package. As detailed herein, we have, therefore, endeavored to implement multiple-walker strategies for calculations into the popular molecular dynamics package NAMD,[33] while continuing to evaluate and improve these strategies.

Within NAMD, the ABF algorithm can be conveniently applied using the Colvars module.[34] Previously, multiple-walker strategies were, however, not implemented in this module. Leveraging tools recently added to NAMD for other replica-exchange algorithms,[23] we have programmed extensions to the Colvars module and NAMD to enable the use of multiple-walker ABF algorithms through a user-friendly interface. We describe herein the implementation of these algorithms in NAMD and further compare them with conventional calculations, highlighting significant advantages in a number of sampling regimes.

THEORETICAL UNDERPINNINGS

When using the ABF algorithm,[5,27,28] diffusion across the transition coordinate can be initially slow because estimates of the mean force are poor or nonexistent in unexplored regions—a situation that can be improved by means of multiple-walker numerical schemes. One communication strategy is characterized by collecting force samples from each walker in a shared buffer—as opposed to having individual buffers for each walker—as the simulations simultaneously progress. This shared buffer is merely conceptual. In practice, we synchronize the force samples among the walkers periodically.

Multiple-walker ABF calculations often yield dramatic improvements over the equivalent calculations with independent walkers.[22] As each walker diffuses randomly along the transition coordinate, it is, however, often the case that several

walkers accumulate samples in neighboring regions, which results in some ranges of the transition coordinate being heavily sampled, while others may be neglected. One possible strategy to increase the efficiency of sampling consists in applying selection rules to the walkers at fixed intervals, eliminating replicas having a value of the transition coordinate in an already well sampled region and duplicating replicas in which a less sampled region is being explored.[2,21,32]

As described in detail below, in this work, application of selection rules is attempted every 50 000 steps, only being applied when the degree of nonuniformity in sampling is above some threshold. The weight assigned to each walker is the inverse of the number of samples that have been accrued in the bin currently occupied by the walker, so that walkers in regions with the least sampling are favored. Specifically, the normalized weight of walker i at the time step of selection is

$$w_t^i = \frac{1}{C_t[n_t(I(q_t^i)) + 1]} \tag{1}$$

where q_t^i is value of the transition coordinate of walker i at time t, the function $I(q)$ maps the transition coordinate to a bin index, and $n_t(b)$ is the is the number of samples accumulated by all walkers in bin b up to time t. The +1 in the denominator ensures that w_t^i is not infinite. The normalization constant is given by $C_t = \sum_{i=0}^{R-1} 1/[n_t(I(q_t^i) + 1)]$, where R is the total number of replicas.

The number of copies of each replica after applying the selection, which can range from 0 to R, is determined according to the weights by a resampling procedure.[21] The following pseudocode summarizes the algorithm utilized to produce copy numbers for each replica, N_t^i, which are guaranteed to be consistent with the constraint $\sum_{i=0}^{R-1} N_t^i = R$.

set $u_t \sim U(0, 1)$, $W_t^0 = w_t^i$, $N_t^0 = \lfloor RW_t^0 + u_t \rfloor$

for $i = 1, ..., R - 1$

$W_t^i = W_t^{i-1} + w_t^i$

$N_t^i = \lfloor RW_t^i + u_t \rfloor - \lfloor RW_t^{i-1} + u_t \rfloor$

end

Here, u is a single pseudorandom number chosen at the beginning of the resampling procedure consistent with a uniform distribution on the domain $[0,1]$.

While the purpose of the selection rules is to improve sampling, a poorly designed selection mechanism can actually spoil good sampling. The worst possible scenario would involve all walkers being deleted except one, which is duplicated R times. Such a situation would negate the advantages of multiple walkers, with phase space effectively being sampled by only a single walker. While the algorithm described above should not lead to such pathological behavior under typical conditions, it may have subtler ill effects on sampling. Notably, the selection rules do not take into account sampling along orthogonal degrees of freedom, which would be quite difficult to correctly and efficiently implement in practice. Under these rules, two walkers with similar values of the transition coordinate can be considered redundant, while, in reality, they may occupy very different values of orthogonal coordinates and, therefore, be sampling disjoint regions of phase space.

To avoid overly aggressive selection and reduce the computational cost of duplication, we cease applying the selection rules when the regions currently occupied by the walkers have sufficiently uniform sampling. Specifically, the selection is disabled during selection time steps t for which

$$\frac{\max_i[n_t(I(q_t^i))] - \min_i[n_t(I(q_t^i))]}{\max_i[n_t(I(q_t^i))]} < \alpha \tag{2}$$

where $\max_i[n_t(I(q_t^i))]$ and $\min_i[n_t(I(q_t^i))]$ give the greatest and least sample counts among the occupied bins and α is a nonnegative real number. The value of α effectively determines how nonuniform the sampling along the transition coordinate may be. Common sense would suggest that the numbers of samples in different regions of the transition coordinate should, at worst, be of the same order of magnitude, which corresponds to $\alpha = 0.9$. On the other hand, differences of 10% or 20% in sampling probably do not justify the loss of diversity caused by eliminating a walker; hence, α should probably be greater than 0.2.

IMPLEMENTATION DETAILS

The Colvars module,[34] available within NAMD, provides a flexible and user-friendly interface for performing calculations. We have, therefore, implemented multiple-walker ABF features in NAMD through extensions of the Colvars module, as well as through the recently implemented replica communication infrastructure within the core of NAMD.[23] Beyond the features described in Jiang et al.,[23] implemention of selection rules requires the additional ability to exchange the state of the simulation system, including atomic coordinates, velocities, and barostat parameters, between replicas.

Simulation state exchange is enabled by two features added to the Tcl scripting interface of NAMD 2.10.[35] First, the simulation state saved to the filesystem with the long-standing output command can now be loaded during a run (rather than only at the beginning) by specifying the file base name to the reinitatoms command. The filesystem allows an arbitrary number of states to be saved and accessed but at a potential performance cost due to the slowness of file writing and reading. Second, the simulation state can be directly transferred between a pair of replicas via the replicaAtomSend, replicaAtomRecv, and replicaAtomSendrecv Tcl commands. These commands are analogous to the replicaSend, replicaRecv, and replicaSendrecv commands used to transfer arbitrary data between replicas and follow the same familiar MPI-style semantics. The direct simulation state transfer commands are designed to be highly scalable, bypassing not only the filesystem but also any single-node bottlenecks by transmitting data directly between corresponding elements of the NAMD spatial decomposition data structures, which are distributed across all nodes of the communicating replicas. This distributed element-wise communication necessitates that the new NAMD option replicaUniformPatchGrids be enabled to ensure compatible data structures on all replicas. In both cases, the exchanging replicas must have identical molecular structures and atom counts.

USING MULTIPLE-WALKER ABF

For flexibility and ease-of-use, the multiple-walker ABF features that we have added to NAMD can be accessed through two complementary interfaces. The simplest way to apply multiple-walker ABF, which should fulfill the needs of some users, is through the inclusion of a few additional keywords in the Colvars[34] configuration file. Examples of the use of these keywords are shown in Figure 1. Adding the shared keyword to

dx.doi.org/10.1021/ct500874p | J. Chem. Theory Comput. XXXX, XXX, XXX−XXX

```
abf {
   name abf1
   colvars endToEnd
   fullSamples 500
   historyFreq 2000
}
```

```
abf {
   name abf2
   colvars endToEnd
   fullSamples 500
   historyFreq 2000
   shared
   sharedFreq 2000
}
```

Figure 1. Segments of a configuration file of the Colvars module, showing usage. (Left) Adaptive biasing force for a single walker or multiple replicas with no inter-replica communication. (Right) Multiple-walker ABF, with samples synchronized among replicas every 2000 steps.

```
set n 10000
set sharedFreq 2000
for {set i 0} {$i < $n} {incr i} {
   run $sharedFreq
   cv bias abf1 share
}
```

```
replicaUniformPatchGrids on
set n 10000
set sharedFreq 2000
for {set i 0} {$i < $n} {incr i} {
   run $sharedFreq
   cv bias abf1 share
   if {$i % 25 == 24} {
       selectionRules
   }
}
```

Figure 2. Segments of a NAMD configuration file, showing usage of multiple-walker ABF through the Tcl interface. (Left) Multiple-walker ABF, with force samples synchronized among replicas every 2000 steps. (Right) Multiple-walker ABF, with force samples synchronized among replicas every 2000 steps and selection rules applied every 50 000 steps. The Tcl procedure selectionRules is defined below.

an ABF (abf) segment of the configuration file is all that is needed to invoke sharing of samples among walkers in a multiple-replica NAMD run. The interval at which synchronization of the force samples occurs defaults to colvarsRestartFreq but can be customized using the new sharedFreq keyword.

A second method to access the multiple-walker ABF features proceeds through the Tcl interface of NAMD, examples of which are shown Figure 2. In addition to permitting an implementation identical to that available through the new commands of the Colvars module, this method gives much greater flexibility, allowing different and more complex sharing and selection protocols to be created, as well as customized output and diagnostics. Samples can be synchronized among all replicas by executing the cv bias <biasName> share command. Selection rules, on the other hand, can be implemented using the new replicaAtomSend and replicaAtomRecv commands, which transfer the complete simulation state between replicas. The selection rules used in this work are a function of the number of samples in the region surrounding each replica; hence, the application of such selection rules should ordinarily be preceded by sample synchronization (e.g., [cv bias abf1 share]), so that the aggregate sample counts over all replicas are available. However, NAMD does not constrain the order in which the Tcl commands are called, and it is up to the user to ensure that the selection rules are applied at the appropriate times.

Here we describe the algorithm implementing the selection rules used in the present work in natural language, with the Tcl code given below. We assume that within the Colvars configuration file, we have defined an instance of the ABF method with the name abf1, as in the left panel of Figure 1. In the NAMD configuration file, the simulation is run for 2000 steps, after which force samples are synchronized among all replicas, using the Tcl command [cv bias abf1 share] on the bias abf1. Each replica extracts the total number of samples that have been collected in the bin it currently occupies, using the [cv bias abf1 bin] and [cv bias abf1 count] commands of the Tcl interface. These numbers are sent to Replica 0, which calculates the weights by eq 1, as well as the minimum and maximum number of samples. Replica 0 determines whether the difference in the maximum and minimum number of samples fulfills the criterion given in eq 2. If the sampling at the current location of the replicas is sufficiently uniform, no sampling occurs and Replica 0 sends an empty list to all walkers. Otherwise, the replicas are resampled according to the algorithm given in "Theoretical Underpinnings," which is represented by the Tcl procedure resampleWalkers in the code below. The definition of resampleWalkers in the Tcl language is given in the Supporting Information. The result of resampleWalkers is a list of the number of copies for each replica (copyNumList). The Tcl procedure minExchanges, also defined in the Supporting Information, then determines which replicas overwrite which other replicas, done in such a way as to minimize the number of system configurations that must be communicated. Essentially, replicas having a copy number of zero are overwritten by those having a copy number of more than one. The result of minExchanges is a list of pairs of replica indices, the first index of the pair being the source replica and the second being the destination replica. Replica 0 then sends this list to all other replicas. Each replica then determines whether it is the source or destination in any of the pairs, and, if so, sends its complete simulation state or receives a new simulation state using the Tcl procedures replicaAtomSend and replicaAtomRecv, respectively. The Tcl code for this algorithm is given as follows—lines prefixed by the pound sign "#" are comments in Tcl.

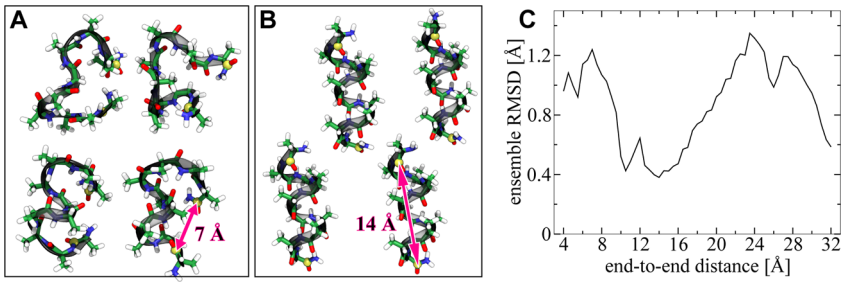

Figure 3. Conformational degeneracy in deca-alanine characterized by its end-to-end distance. (A) Typical conformations for an end-to-end distance of 7.0 Å. (B) Typical conformations for an end-to-end distance of 14.0 Å. In the renderings, the carbonyl carbon atoms used to define the end-to-end distance are shown as yellow spheres. Hydrogen, carbon, nitrogen, and oxygen atoms are colored white, green, blue, and red, respectively. (C) Root-mean-square deviation (RMSD) of atomic positions for conformational ensembles at different values of the end-to-end distance. The RMSD is computed between all pairs of conformations observed at each distance value and these are then averaged.

```
proc selectionRules {} {
# Get the count of the walker's bin.
set binNum [cv bias abf1 binnum]
set bin [cv bias abf1 bin]
if {$bin < 0} { set bin 0 }
if {$bin >= $binNum} {set bin [expr {$binNum-1}]}
set count [cv bias abf1 count $bin]

replicaBarrier; # Synchronize.
if {[myReplica] > 0} {
   # Send the count to Replica 0.
   replicaSend $count 0
   # Receive indices of source/dest replicas.
   set srcDestList [replicaRecv 0]
} else {
    # My replica is Replica 0.
    # Gather other replicas' counts.
    set w [expr {1.0/($count+1)}]
    set wList [list $w]
    set cMin $count; set cMax $count
    for {set r 1} {$r < [numReplicas]} {incr r} {
        set c [replicaRecv $r]
        if {$c < $cMin} { set cMin $c }
        if {$c > $cMax} { set cMax $c }
        set w [expr {1.0/($c+1)}]
        lappend wList $w
    }
    # Disable selection?
    set relDif [expr (double($cMax-$cMin))/$cMax]
    if {$relDif < 0.4} {
        set srcDestList {}
    } else {
        # Resample the walkers
        set copyNumList [resampleWalkers $wList]
        # Make a list of src and dest replicas.
        set srcDestList [minExchanges $copyNumList]
    }

    # Replica 0 sends the src and dest replicas
    # to all other replicas.
    for {set r 1} {$r < [numReplicas]} {incr r} {
        replicaSend $srcDestList $r
    }
 }; # End else, Replica 0 work

# All replicas have an identical 'srcDestList'.
# Send or receive the atomic system if in list.
print "(SelectionRules) $srcDestList"
foreach {src dest} $srcDestList {
    if {$src == [myReplica]} {
        replicaAtomSend $dest
    } elseif {$dest == [myReplica]} {
        replicaAtomRecv $src
    }
}
}; # End proc selectionRules
```

METHODOLOGICAL DETAILS

To evaluate the performance of the implemented multiple-walker strategies, molecular dynamics simulations of deca-alanine in vacuum[28,36] were performed using NAMD 2.10.[33] The atomic interactions were defined by the CHARMM22 force field for proteins with CMAP corrections.[37,38] The Langevin equations of motion were integrated with a 2 fs time step, a temperature of 300 K, and a damping constant of 1 ps^{-1}, using the scheme of Brünger, Brooks, and Karplus.[39] The simulations were performed in vacuum, and both electrostatic and van der Waals energies were smoothly truncated to zero between 10 and 12 Å. Covalent bonds involving hydrogen atoms were constrained using the RATTLE algorithm.[40]

The ABF method[5,27,28] was employed along a transition coordinate defined as the Euclidean distance between the carbon atoms of the first and last carbonyl groups of deca-alanine. Instantaneous-force statistics were collected in 0.1 Å bins along the transition coordinate on the domain 4−32 Å. For each interval of the transition coordinate, the biasing force was applied once a minimum of 500 samples were accrued in the corresponding bin. Where indicated, multiple-walker ABF was applied at 2000-step (4 ps) intervals and selection rules were applied at 50 000-step (100 ps) intervals.

RESULTS AND DISCUSSION

In this section, we first describe some properties of the model system used in this work that are relevant to the convergence of the multiple-walker ABF strategies. We then apply these strategies to the model system with two distinct domains of the transition coordinate, first excluding and then including the most difficult region to sample. We compare the performance of the different strategies in terms of both real time and computational cost, as well as how reliably they appear to converge to the correct solution. Over the first domain, that is, 12−32 Å, we find that a ten-walker protocol, with or without selection rules, yields rapid convergence—approximately ten times faster in real time than a single walker—while having the same computational cost. Conversely, for the second domain, that is, 4−32 Å, all multiple-walker schemes yield better performance, considering both real time and computational cost. While the single-walker calculation and the multiple-walker ABF calculation with selection rules admittedly display

dx.doi.org/10.1021/ct500874p | J. Chem. Theory Comput. XXXX, XXX, XXX−XXX

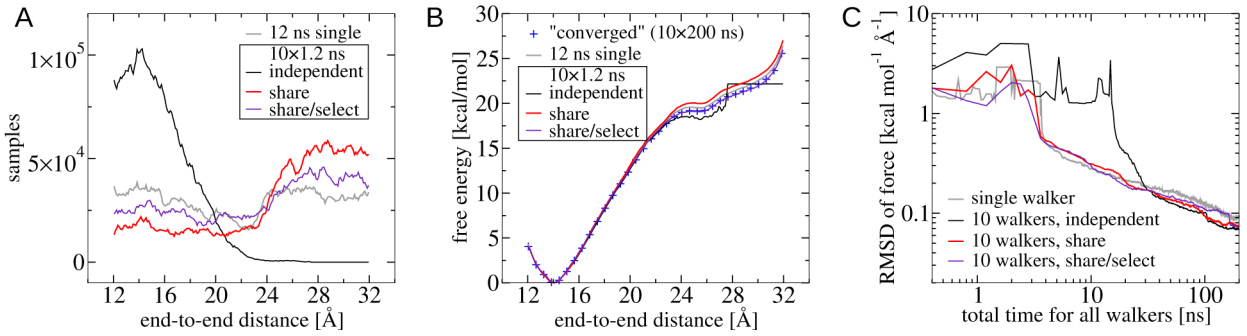

Figure 4. Convergence of ABF for deca-alanine on the 12−32 Å domain. (A) Number of force samples gathered by the algorithm in a total of 12 ns of simulated time. "Single," "independent," "share," and "share/select" refer respectively to a single 12 ns calculation, ten independent 1.2 ns multiple-walker ABF calculations, ten 1.2 ns calculations, and ten 1.2 ns calculations with selection rules applied periodically. See text for the full detail of the protocols. (B) Free-energy estimates after a total of 12 ns of simulated time. For reference, a converged profile obtained by averaging the results of ten independent simulations, each 200 ns in length, is represented by blue crosses. (C) Convergence: Root-mean-square deviation (RMSD) from the converged mean force profile as a function of total simulated time. Note that, given sufficient computational resources, the ten-walker simulations can be run ten times faster than the single-walker simulation.

sluggish and unreliable convergence on the difficult region of the domain, multiple-walker ABF by itself shows more than an order of magnitude faster convergence in both the short- and long-time regimes.

PROPERTIES OF THE MODEL SYSTEM

Just as in previous work,[5,8,21,28] we employ the reversible unfolding of the ten amino-acid peptide deca-alanine as a model system. While we consider this peptide in vacuum, note that recent simulations have shown a somewhat more complicated free-energy landscape in water.[41]

The Euclidean end-to-end distance of the peptide chain, ξ, serves as a convenient and intuitive transition coordinate for describing folding and unfolding. Yet, despite the apparent simplicity of deca-alanine and the obviousness of the choice of the transition coordinate, estimation of the free energy for the compact region, $\xi \in [4, 10]$ Å, is severely thwarted by hidden barriers.[8,21] For example, as depicted in Figure 3A, many qualitatively different conformations corresponding to $\xi = 7$ Å can be observed in the course of the simulation. Conversely, as shown in Figure 3B, conformations observed for $\xi = 14$ Å all possess a similar α-helical form, with the largest conformational diversity occurring near the termini of the peptide chain.

The extent of conformational degeneracy for a given range of ξ values was characterized by computing the root-mean-square deviation (RMSD) between all pairs of conformations observed in simulations within 0.01 Å of a given value of the end-to-end distance, with rigid transformations applied to minimize each RMSD. The means of these RMSD values for each value of ξ are summarized in Figure 3C, where the data was derived from a multiple-walker ABF calculation consisting of ten walkers, each simulated for 100 ns. Smaller values of the mean-ensemble RMSD imply low conformational degeneracy, akin to the neighborhood of $\xi = 14$ Å, where the α-helical conformation is overwhelmingly dominant. Conversely, the plot implies large conformational degeneracy for compact conformations ($\xi < 9$ Å), as well as for partially extended helices ($20 < \xi < 30$ Å). Particular difficulty in obtaining convergence of the potential of mean force along ξ has been noted in these two regions of the transition coordinate.[5,8,21] Conformational degeneracy does not by itself pose difficulties for estimating the free energy along ξ; however, when distinct conformations of similar free energies are separated by sizable free-energy barriers—or subject to slow kinetics—properly sampling the conformations within the limited time of typical molecular dynamics simulations becomes problematic. The hidden barriers are particularly large for compact conformations of deca-alanine, such as those shown in Figure 3A, where steric effects prevent smooth transitions between them.

CONVERGENCE ON THE 12−32 Å DOMAIN

We begin by considering the behavior of the multiple-walker algorithms on the easier 12−32 Å domain of the transition coordinate. The behavior on this domain is simpler than that on the 4−32 Å domain and serves as a basis to understand the results for the latter. We compare four different strategies in the calculations, namely a single walker, ten independent walkers, ten walkers sharing force samples every 2000 steps (4 ps), and ten walkers with the same sharing frequency and selection rules applied every 50 000 steps (100 ps). The variable α that determined whether the selection rules were actually applied, according to eq 2, is 0.4. Other values of α, including 0.2, 0.6, and 0.8, were considered. $\alpha = 0.2$ appeared to reduce the rate of convergence relative to $\alpha = 0.4$, while for $\alpha = 0.8$, the selection rules were never applied. We have chosen the frequencies of sharing and applying selection rules such that the relative computational burden of sharing and selection rule application is small—the simulation efficiency (in ns/day) is no less than 90% of that for independent walkers. Thus, the computational cost of a single walker running for 10 ns or ten walkers running for 1 ns, using any communication scheme, have roughly the same computational cost. In the plots of Figure 4, we make comparisons based on similar computational cost. It is, however, important to note that, given sufficient computational resources, the real time required for a single walker is roughly ten times that required for any of the multiple-walker schemes. To make best use of the data extracted from independent walkers, at the end of the calculations, we compute the mean forces over all walkers by

$$\langle F(\xi_b)\rangle = \frac{\sum_{i=0}^{R-1} n_i^b \langle F_i(\xi_b)\rangle}{\sum_{i=0}^{R-1} n_i^b} \tag{3}$$

where ξ_b is the center of the bin b along the transition coordinate ξ, n_i^b is the number of force samples collected by walker i in bin b, and $F_i(\xi_b)$ is the mean force calculated in bin b

dx.doi.org/10.1021/ct500874p | J. Chem. Theory Comput. XXXX, XXX, XXX−XXX

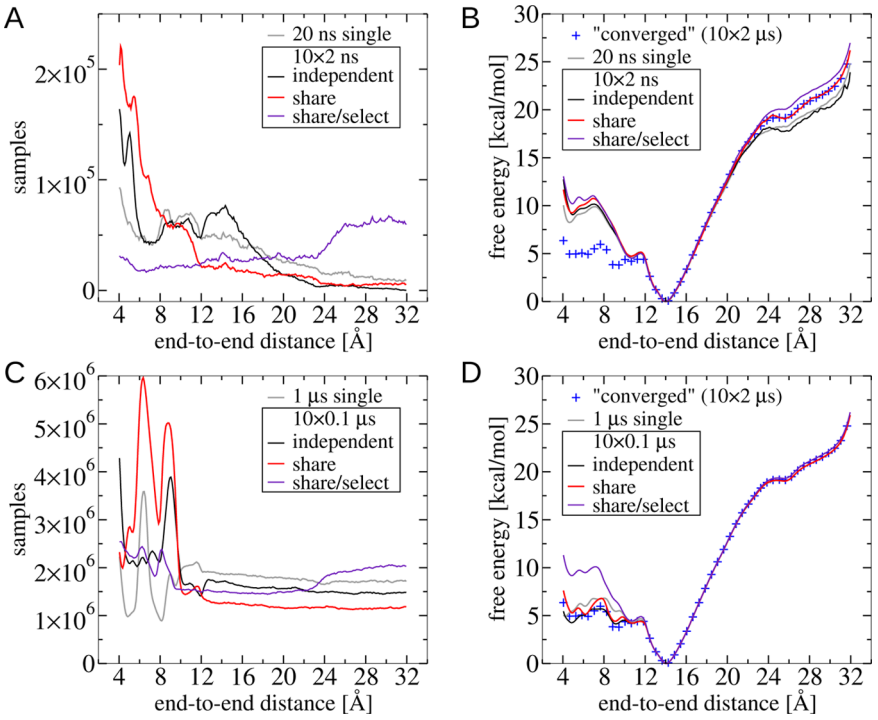

Figure 5. ABF calculation for deca-alanine on the 4−32 Å domain. (A) Number of force samples gathered by the ABF algorithm in a total of 20 ns of simulated time. "Single," "independent," "share," and "share/select" refer respectively to a single 20 ns ABF calculation, ten independent 2 ns calculations, ten 2 ns multiple-walker ABF calculations, and ten 2 ns multiple-walker ABF calculations with selection rules applied periodically. See text for full details on the protocol. (B) Free energy estimates after a total of 20 ns of simulated time. For reference, a converged profile obtained by averaging the results of ten independent simulations, each 2 μs in length, is represented by blue crosses. (C) Number of force samples gathered by the algorithm in a total of 1 μs of simulated time. (D) Free energy estimates after a total of 1 μs of simulated time.

for walker i. To analyze the quality of sampling, the counts of samples for all walkers can simply be summed, that is, $n^b = \sum_{i=0}^{R-1} n_i^b$. When the multiple-walker ABF algorithm is employed, the samples are combined periodically within NAMD during the calculations, obviating the need to merge them a posteriori.

The first important issue is whether the walkers are able to quickly explore the entire domain, as no information on free-energy differences can be obtained in regions of the transition coordinate that have not been sampled hitherto. In all cases, the starting conformation is the α-helix, which corresponds to the free-energy minimum and to an end-to-end distance of about 14 Å. Some time is required for the systems to diffuse away from this minimum and explore more of the domain—a process that is mainly limited by the rate at which the ABF algorithm can accrue samples in previously unexplored regions. Figure 4A shows the number of force samples, n^b, collected by the algorithm in bin b after a total of 12 ns of simulated time, which, for the multiple-walker algorithms, corresponds to ten walkers simulated over 1.2 ns each. From this plot, it is clear that the rate of exploration is subservient to the communication strategy. Within 12 ns, the single walker is able to sample the whole domain in a relatively uniform fashion. If we ignore the fact that the single-walker calculation may require 10-fold more real time, the combined sampling of ten independent walkers in 1.2 ns is relatively poor—few samples have been collected far away from the initial position and no samples have been obtained for ξ > 27.6 Å. Sharing samples among the walkers, however, allows the transition coordinate to be explored much more rapidly. Both calculations with the multiple-walker ABF protocol were able to sample the entire domain relatively uniformly in <1.2 ns, with the selection rules yielding slightly more uniform sampling.

The potentials of mean force derived from 12 ns single-walker and 1.2 ns multiple-walker calculations are shown in Figure 4B. Due to the poor sampling evident in Figure 4A, the calculation consisting of ten independent walkers does not give a good representation of the potential of mean force for ξ > 22 Å, with the flat region for ξ > 27.6 Å associated with no sampling at all. The other three calculations give deviations from the converged curve of <1 kcal/mol over the entire domain, with the best agreement resulting from multiple-walker ABF with selection rules. Thus, in about one-tenth of the real time at almost no additional computational cost, multiple-walker ABF with ten walkers can give potentials of mean force nearly as good, or even better than a single walker.

As has been noted previously,[22] convergence of ABF calculations can be roughly delineated into two phases. At the beginning of the calculation, the effective free-energy landscape remains rugged, either because few force samples have been gathered and the biasing force is not yet applied, or because the biasing force is inaccurate and does not adequately remove free-energy barriers. In this first phase, exploration of the transition coordinate is limited by remnant barriers in the effective free-energy surface, that is, the intrinsic free-energy surface plus the biasing potential. Once the biasing force becomes sufficiently accurate—that is, when the biasing potential deviates from the negative of the real potential of mean force by less than $k_B T$—the effective free-energy landscape, including the effect of the biasing force, is sufficiently flat that the system freely diffuses along the transition

dx.doi.org/10.1021/ct500874p | J. Chem. Theory Comput. XXXX, XXX, XXX−XXX

coordinate. Note that when exploration is slow, these phases may occur at different times for different subdomains.

The overall convergence properties of the calculations for the 12−32 Å domain can be seen in Figure 4C, which plots the root-mean-square deviation of the estimated mean force from the converged mean force as a function of time. The converged mean force was obtained by averaging the results inferred from ten independent walkers simulated for a total time of 2 μs. The two phases described in the last paragraph can be clearly observed. In all cases, the estimated mean forces fluctuate considerably with respect to the converged mean force early in the calculation. After a time that depends on the communication strategy, the fluctuations decrease and the estimated mean forces rapidly and uniformly approach the converged values. The deviations are then comparable among the protocols and seem to converge at a similar rate, although the single walker seems to lag slightly behind the others. Approximately 4 ns is required for the single walker to begin converging smoothly. The ten independent walkers reach a smooth-convergence regime in less real time, albeit at a greater computational cost, requiring about 3 ns per walker or 30 ns total. However, for an equal computational cost and about one-tenth of the real time, the multiple-walker ABF calculations give similar or superior convergence relative to a single walker. Note that, due to the criterion in eq 2, the selection rules were applied nearly every 0.1 ns until the total time for all walkers reached 16 ns, after which time sampling became sufficiently uniform that application of the selection rules ceased.

To characterize the rate of convergence, we performed least-squares fits to a power law on the curves in Figure 4C. We considered only the behavior of the error after the initial transient, that is, for total times t > 39 ns for the independent-walker calculation and t > 4.5 ns for all other calculations. The exponents, ranging from −0.37 for a single walker to −0.49 for multiple-walker ABF without selection rules, were similar to those expected for averages over a stochastic process, where the error is $\sim 1/\sqrt{t}$.

CONVERGENCE ON THE 4−32 Å DOMAIN

The results in the last section demonstrated that, for a relatively well behaved system, the multiple-walker ABF algorithm can yield convergence of the free energies for the same computational cost as a single walker in much less real time. However, the advantage of the multiple-walker ABF protocol becomes most clear for systems wherein convergence is more difficult to achieve. In the case of the reversible unfolding of deca-alanine on the 4−32 Å domain, we find that, in addition to reducing the real time necessary for a calculation, the multiple-walker ABF algorithm also reduces the computational cost and enhances the reliability of the result.

Figure 5A shows the samples in each 0.1 Å bin for a 20 ns single-walker calculation and ten-walker calculations with 2 ns per walker. Except for the calculation using selection rules, all calculations show a tendency to accumulate a large number of samples for ξ < 6 Å. While the selection rules guarantee that the sampling be more uniform, as we will see shortly, this may not be beneficial. In all cases, as revealed in Figure 6B, a total simulation time of 20 ns over all walkers is not sufficient to obtain convergence for the compact ξ < 10 Å region.

The plots of Figure 5C and D show the number of samples per bin together with the estimated potentials of mean force for free-energy calculations totaling 1 μs of simulation time. We continue to see substantially nonuniform sampling for all

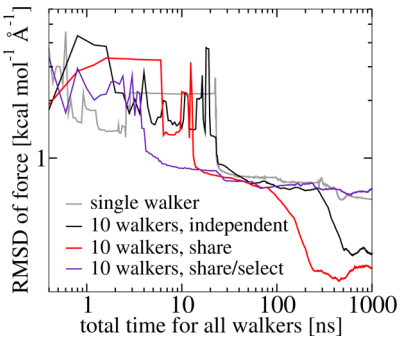

Figure 6. Convergence of the ABF simulation for deca-alanine on the 4−32 Å domain, as indicated by the root mean-square deviation of the estimated mean forces from the converged force profile as a function of total simulated time.

calculations devoid of selection rules, as highlighted in Figure 5C. For reasons that are not completely clear, multiple-walker ABF shows large peaks in sampling at ξ = 6.4 and 8.8 Å—this lack of sampling uniformity likely stems from limitations in the ability of a one-dimensional transition coordinate to distinguish between compact conformations of the peptide chain corresponding to nearly identical free energies. Smaller peaks at similar locations are seen for the single walker and independent walkers, with additional peaks as ξ approaches 4 Å. The overabundance of instantaneous-force samples for ξ < 10 Å seems to reflect a better convergence on this interval, as the calculations with independent walkers and multiple-walker ABF alone, which have the greatest preponderance of samples in this region, also have the best correspondence with the reference potential of mean force (see Figure 5D). Indeed, after 1 μs of total simulation time, the potential of mean force for multiple-walker ABF with selection rules is almost identical to that at 20 ns, which may be explained by an adverse effect of the selection rules, which by ensuring uniform sampling prevent important conformations of the free-energy landscape in the region of ξ < 10 Å to be explored appropriately. It is interesting to note that, due to the criterion in eq 2, the selection rules were applied frequently at the beginning of the free-energy calculation, but only rarely after 100 ns of the total simulation time. Specifically, the selection rules were enabled in 75% of the selection intervals before 100 ns, but only 14% afterward. Therefore, after 100 ns, the average time between application of the selection rules was about 700 ps.

Figure 6 shows the root mean-square deviation of the estimated mean forces from the converged mean forces, which were derived from a calculation of independent walkers totaling 20 μs of simulated time. Here, we can see that the convergence of independent walkers and multiple-walker ABF alone appears to have transpired in discrete steps. Reasonably good convergence in the [4, 10] Å region was found only after about 200 ns of simulation over all walkers for multiple-walker ABF alone, and after about 400 ns for independent walkers. On the other hand, the single walker and multiple-walker ABF with selection rules seem to never attain this level of convergence in the limited time of the free-energy calculations.

In stark contrast with the results accrued for the 12−32 Å domain, here, the single-walker strategy is clearly the worst performer, even when considering only the computational cost and neglecting the greater real time required for a single-walker calculation. The short-time convergence is also much poorer than for the calculation in terms of both real time and

computational cost. Most worrisome is the fact that the mean force never appears to properly converge in the [4, 10] Å region during the free-energy calculation. While the multiple-walker ABF simulation with selection rules has a much better short-time convergence, it also appears to have similar long-time convergence problems.

It seems that although the nonuniform sampling seen in Figure 6A and C for the case without selection rules could naively be viewed as wasteful, it may be necessary to spend a larger amount of time in the $4 < \xi < 10$ Å region to obtain proper sampling of the many compact conformations of the peptide chain, such as those depicted in Figure 3A. It may be for this reason that multiple-walker ABF without selection rules is the best performer in the long-time regime.

CONCLUSION

Conventional molecular simulations relying upon Boltzmann sampling are plagued by the well-known multiple-minima problem, which is rooted in the pronounced ruggedness of the free-energy landscape, common, among others, to many biological objects, and which causes sampling to become kinetically trapped in one local minimum amidst an overwhelmingly huge number of local, low free-energy states. Harnessing the formidable computing potential of large, massively parallel architectures, multiple-replica paradigms offer a convenient framework to overcome this difficulty by exploring concomitantly on different processing units a wide range of conformational space and exchanging information periodically. Employing the replica-communication infrastructure developed in the popular molecular dynamics program NAMD,[33] we describe in the present work the implementation of one such paradigm, referred to as multiple-walker ABF, and assess in a systematic fashion the performance of the algorithm in a series of simulations on the prototypical peptide chain deca-alanine in vacuum.[28,36] In a nutshell, multiple-walker ABF is a multiple-walker extension of the importance-sampling approach ABF,[5,27,28] an algorithm which, in the course of the simulation, estimates locally the required biasing force to yield a Hamiltonian bereft of an average force acting along the transition coordinate. Applicability of the algorithm is subservient in large measure to time scale separation and how decoupled the chosen transition coordinate is from other degrees of freedom in the slow manifold. In practice, for a large variety of geometrical transformations, sampling is often hampered by hidden, virtually insurmountable free-energy barriers in the direction orthogonal to the transition coordinate—a common shortcoming of oversimplifying the representation of the reaction coordinate by means of a one-dimensional order parameter. Multiple-walker ABF addresses this shortcoming by populating the many valleys of the free-energy landscape separated by high barriers, exchanging periodically information about the local force felt by the different walkers. The proposed numerical scheme can be further sophisticated by applying a Darwinian selection to the replicas, spawning the walkers that have covered large portions of the transition coordinate, while eliminating the less effective ones. Application of the methodology to the toy model of deca-alanine in vacuum reveals that the multiple-walker ABF algorithm improves ergodic sampling and systematically outperforms strategies wherein replicas explore the free-energy landscape independently—let alone single-walker strategies. Furthermore, application of walker selection rules enhances sampling uniformity and accelerates short-time convergence but shows adverse effects over longer simulation times, from whence one might be tempted to infer that enforcement of sampling uniformity may not be the best possible choice. In the light of this somewhat counterintuitive behavior, we suggest that selection rules be only applied in the early stage of the simulation, turning to the standard implementation of the multiple-walker ABF algorithm thereafter. Indeed, progressive reduction of the selection rate has already been suggested in Section 6.2.1.2 of ref 2. The ease of implementation of the multiple-walker strategies for the method described herein, notably through the replica-communication infrastructure available in NAMD, is suggestive of many alternate protocols and possible extensions, chief among which is simultaneous multiple-walker ABF and parallel tempering. In the latter, several sets of walkers would be simulated with each set at a different temperature. Walkers at the same temperature would communicate force samples, maintaining a synchronized shared buffer of force samples for each temperature, while exchanges of configurations between different temperatures would be performed according to the Metropolis–Hastings criterion. An efficient implementation could prove useful to estimate the entropy changes that accompany geometric transformations and is currently underway in NAMD, guided by earlier encouraging results on chemical and biological model systems.[22]

ASSOCIATED CONTENT

Supporting Information

Tcl implementation of the procedures resampleWalkers and minExchanges used by the procedure selectionRules. This material is available free of charge via the Internet at http://pubs.acs.org.

AUTHOR INFORMATION

Corresponding Author

*E-mail: chipot@ks.uiuc.edu.

Notes

The authors declare no competing financial interest.

ACKNOWLEDGMENTS

The authors acknowledge useful input from Dr. Jérôme Hénin, Institut de Biologie Physico-Chimique in Paris, and Dr. Giacomo Fiorin, Institute for Computational Molecular Science, Philadelphia, for the implementation of the code in the Colvars module. They are equally indebted to Nikhil Jain and Laxmikant Kalé, Department of Computer Science, University of Illinois at Urbana–Champaign, for fruitful discussions on the replica-exchange communication infrastructure within NAMD. They are grateful to the Grand Équipement National de Calcul Intensif, Centre Informatique National de l'Enseignement Supeérieur in Montpellier, and the Partnership for Advanced Computing in Europe program for generous allocation of computer time.

REFERENCES

(1) Chipot, C.; Pohorille, A. *Free Energy Calculations*; Springer: Berlin, 2007.

(2) Lelièvre, T.; Stoltz, G.; Rousset, M. *Free Energy Computations: A Mathematical Perspective*; World Scientific: Singapore, 2010.

(3) Chipot, C. Frontiers in Free-Energy Calculations of Biological Systems. *Wiley Interdiscip. Rev. Comput. Mol. Sci.* **2014**, *4*, 71–89.

(4) Gumbart, J. C.; Roux, B.; Chipot, C. Standard Binding Free Energies from Computer Simulations: What Is the Best Strategy? *J. Chem. Theory Comput.* **2012**, *9*, 794−802.
(5) Comer, J.; Gumbart, J. C.; Hénin, J.; Lelièvre, T.; Pohorille, A.; Chipot, C. *J. Phys. Chem. B*, **2014**, DOI 10.1021/ct500874p.
(6) Best, R.; Hummer, G. Reaction Coordinates and Rates from Transition Paths. *Proc. Natl. Acad. Sci. U.S.A.* **2005**, *102*, 6732.
(7) Dehez, F.; Tarek, M.; Chipot, C. Energetics of Ion Transport in a Peptide Nanotube. *J. Phys. Chem. B* **2007**, *111*, 10633−10635.
(8) Hénin, J.; Fiorin, G.; Chipot, C.; Klein, M. Exploring Multidimensional Free Energy Landscapes Using Time-Dependent Biases on Collective Variables. *J. Chem. Theory Comput.* **2009**, *6*, 35−47.
(9) Romo, T. D.; Grossfield, A. Unknown Unknowns: The Challenge of Systematic and Statistical Error in Molecular Dynamics Simulations. *Biophys. J.* **2014**, *106*, 1553−1554.
(10) Zheng, L.; Chen, M.; Yang, W. Random Walk in Orthogonal Space to Achieve Efficient Free-energy Simulation of Complex Systems. *Proc. Natl. Acad. Sci. U.S.A.* **2008**, *105*, 20227−20232.
(11) Shaw, D. E.; Dror, R. O.; Salmon, J. K.; Grossman, J. P.; Mackenzie, K. M.; Bank, J. A.; Young, C.; Deneroff, M. M.; Batson, B.; Bowers, K. J.; Chow, E.; Eastwood, M. P.; Ierardi, D. J.; Klepeis, J. L.; Kuskin, J. S.; Larson, R. H.; Lindorff-Larsen, K.; Maragakis, P.; Moraes, M. A.; Piana, S.; Shan, Y.; Towles, B. Millisecond-Scale Molecular Dynamics Simulations on Anton. In *Proceedings of the Conference on High Performance Computing Networking, Storage and Analysis; SC '09*; ACM: New York, 2009; pp 39:1−39:11.
(12) Zheng, L.; Chen, M.; Yang, W. Simultaneous Escaping of Explicit and Hidden Free Energy Barriers: Application of the Orthogonal Space Random Walk Strategy in Generalized Ensemble Based Conformational Sampling. *J. Chem. Phys.* **2009**, *130*, 234105.
(13) Zheng, L.; Yang, W. Practically Efficient and Robust Free Energy Calculations: Double-Integration Orthogonal Space Tempering. *J. Chem. Theory Comput.* **2012**, *8*, 810−823.
(14) Sugita, Y.; Okamoto, Y. Replica-Exchange Molecular Dynamics Method for Protein Folding. *Chem. Phys. Lett.* **1999**, *314*, 141−151.
(15) Sugita, Y.; Kitao, A.; Okamoto, Y. Multidimensional Replica-Exchange Method for Free-Energy Calculations. *J. Chem. Phys.* **2000**, *113*, 6042−6051.
(16) Woods, C. J.; Essex, J. W.; King, M. A. The Development of Replica-Exchange-Based Free-Energy Methods. *J. Phys. Chem. B* **2003**, *107*, 13703−13710.
(17) Babin, V.; Roland, C.; Sagui, C. Adaptively Biased Molecular Dynamics for Free Energy Calculations. *J. Chem. Phys.* **2008**, *128*, 134101.
(18) Faraldo-Gómez, J. D.; Roux, B. Characterization of Conformational Equilibria through Hamiltonian and Temperature Replica-Exchange Simulations: Assessing Entropic and Environmental Effects. *J. Comput. Chem.* **2007**, *28*, 1634−1647.
(19) Fajer, M.; Swift, R. V.; McCammon, J. A. Using Multistate Free Energy Techniques to Improve the Efficiency of Replica Exchange Accelerated Molecular Dynamics. *J. Comput. Chem.* **2009**, *30*, 1719−1725.
(20) Jiang, W.; Roux, B. Free Energy Perturbation Hamiltonian Replica-exchange Molecular Dynamics (FEP/H-REMD) for Absolute Ligand Binding Free Energy Calculations. *J. Chem. Theory Comput.* **2010**, *6*, 2559−2565.
(21) Minoukadeh, K.; Chipot, C.; Lelièvre, T. Potential of Mean Force Calculations: A Multiple-walker Adaptive Biasing Force Approach. *J. Chem. Theory Comput.* **2010**, *6*, 1008−1017.
(22) Comer, J.; Roux, B.; Chipot, C. Achieving Ergodic Sampling Using Replica-Exchange Free-Energy Calculations. *Mol. Sim.* **2014**, *40*, 218−228.
(23) Jiang, W.; Phillips, J. C.; Huang, L.; Fajer, M.; Meng, Y.; Gumbart, J. C.; Luo, Y.; Schulten, K.; Roux, B. Generalized Scalable Multiple Copy Algorithms for Molecular Dynamics Simulations in NAMD. *Comput. Phys. Commun.* **2014**, *185*, 908−916.
(24) Swendsen, R. H.; Wang, J.-S. Replica Monte Carlo Simulation of Spin Glasses. *Phys. Rev. Lett.* **1986**, *57*, 2607−2609.
(25) Marinari, E.; Parisi, G. Simulated Tempering: A New Monte Carlo Scheme. *Europhys. Lett.* **1992**, *19*, 451.
(26) Lyubartsev, A.; Martsinovski, A.; Shevkunov, S.; Vorontsov-Velyaminov, P. New Approach to Monte Carlo Calculation of the Free Energy: Method of Expanded Ensembles. *J. Chem. Phys.* **1992**, *96*, 1776−1783.
(27) Darve, E.; Pohorille, A. Calculating Free Energies Using Average Force. *J. Chem. Phys.* **2001**, *115*, 9169−9183.
(28) Hénin, J.; Chipot, C. Overcoming Free Energy Barriers Using Unconstrained Molecular Dynamics Simulations. *J. Chem. Phys.* **2004**, *121*, 2904−2914.
(29) Rodriguez-Gomez, D.; Darve, E.; Pohorille, A. Assessing the Efficiency of Free Energy Calculation Methods. *J. Chem. Phys.* **2004**, *120*, 3563.
(30) Lelièvre, T.; Rousset, M.; Stoltz, G. Long-time Convergence of an Adaptive Biasing Force Method. *Nonlinearity* **2008**, *21*, 1155.
(31) Lelievre, T.; Minoukadeh, K. Long-time Convergence of an Adaptive Biasing Force Method: The Bi-channel Case. *Archive for Rational Mechanics and Analysis* **2011**, *202*, 1−34.
(32) Lelièvre, T.; Rousset, M.; Stoltz, G. Computation of Free Energy Profiles with Parallel Adaptive Dynamics. *J. Chem. Phys.* **2007**, *126*, 134111.
(33) Phillips, J. C.; Braun, R.; Wang, W.; Gumbart, J.; Tajkhorshid, E.; Villa, E.; Chipot, C.; Skeel, R. D.; Kale, L.; Schulten, K. Scalable Molecular Dynamics with NAMD. *J. Comput. Chem.* **2005**, *26*, 1781−1802.
(34) Fiorin, G.; Klein, M. L.; Hénin, J. Using Collective Variables to Drive Molecular Dynamics Simulations. *Mol. Phys.* **2013**, *111*, 3345−3362.
(35) Bhandarkar, M.; Bhatele, A.; Bohm, E.; Brunner, R.; Buelens, F.; Chipot, C.; Dalke, A.; Dixit, S.; Fiorin, G.; Freddolino, P.; Grayson, P.; Gullingsrud, J.; Gursoy, A.; Hardy, D.; Harrison, C.; Hénin, J.; Humphrey, W.; Hurwitz, D.; Krawetz, N.; Kumar, S.; Kunzman, D.; Lai, J.; Lee, C.; McGreevy, R.; Mei, C.; Nelson, M.; Phillips, J.; Sarood, O.; Shinozaki, A.; Tanner, D.; Wells, D.; Zheng, G.; Zhu, F. *NAMD User's Guide*, Version 2.10b1. Theoretical and Computational Biophysics Group: University of Illinois at Urbana-Champaign and Beckman Institute: Urbana, IL, 2014.
(36) Park, S.; Şener, M. K.; Lu, D.; Schulten, K. Reaction Paths Based on Mean First-Passage Times. *J. Chem. Phys.* **2003**, *119*, 1313−1319.
(37) MacKerell, A. D., Jr.; Bashford, D.; Bellott, M.; Dunbrack, R. L., Jr.; Evanseck, J.; Field, M. J.; Fischer, S.; Gao, J.; Guo, H.; Ha, S.; Joseph, D.; Kuchnir, L.; Kuczera, K.; Lau, F. T. K.; Mattos, C.; Michnick, S.; Ngo, T.; Nguyen, D. T.; Prodhom, B.; Reiher, I. W. E.; Roux, B.; Schlenkrich, M.; Smith, J.; Stote, R.; Straub, J.; Watanabe, M.; Wiorkiewicz-Kuczera, J.; Yin, D.; Karplus, M. All-Atom Empirical Potential for Molecular Modeling and Dynamics Studies of Proteins. *J. Phys. Chem. B* **1998**, *102*, 3586−3616.
(38) MacKerell, A., Jr.; Feig, M.; Brooks, C., III Improved Treatment of the Protein Backbone in Empirical Force Fields. *J. Am. Chem. Soc.* **2004**, *126*, 698−699.
(39) Brünger, A. T.; Brooks, C. L., III; Karplus, M. Stochastic Boundary Conditions for Molecular Dynamics Simulations of ST2 Water. *Chem. Phys. Lett.* **1984**, *105*, 495−498.
(40) Andersen, H. Rattle: A "Velocity" Version of the Shake Algorithm for Molecular Dynamics Calculations. *J. Comput. Phys.* **1983**, *52*, 24−34.
(41) Hazel, A.; Chipot, C.; Gumbart, J. C. Thermodynamics of Deca-alanine Folding in Water. *J. Chem. Theory Comput.* **2014**, *10*, 2836−2844.